Optical properties of Nd3+-doped TeO2-TiO2-ZnO glasses with lower hydroxyl content

Jonathan de Clermont-Gallerande, Shunsuke Saito, Tomokatsu Hayakawa, Maggy Colas, Philippe Thomas, Jean-René Duclère

Optical properties of Nd^{3+}-doped TeO_2-TiO_2-ZnO glasses with lower hydroxyl content

Jonathan de Clermont-Gallerande[1,2], Shunsuke Saito[1], Tomokatsu Hayakawa[1,3]*, Maggy Colas[2], Jean-René Duclère[2], Philippe Thomas[2]

[1]Field of Advanced Ceramics, Department of Life Science and Applied Chemistry,

Nagoya Institute of Technology, Gokiso, Showa, Nagoya 466-8555, Japan

[2]Institut de recherche sur les céramiques (IRCER), UMR 7315 CNRS / Université de Limoges, Centre Européen de la Céramique, 12, rue Atlantis, 87068 Limoges, France

[3]Frontier Research Institute of Materials Science (FRIMS), Nagoya Institute of Technology, Gokiso, Showa, Nagoya 466-8555, Japan

*corresponding author: hayatomo@nitech.ac.jp

TEL/FAX: +81-52-735-5110

This paper describes Nd^{3+}-ions doped multicomponent tellurite glasses TeO_2-TiO_2-ZnO (TTZ) applicable to advanced optical devices, which were characterized by UV-Vis-NIR absorption, Raman, and photoluminescence (PL) techniques. Not only did we perform experimental characterizations but also theoretically predicted the PL properties of Nd^{3+}-doped TTZ glasses by using the Judd-Ofelt theory. The influence of the residual hydroxyl (OH) groups and types of crucible used in the melt preparation on the structures and optical properties of TTZ glasses was investigated. We found that the use of a Pt crucible increased the network-connecting structures of trigonal bipyramidal TeO_4 compared to the case of a Al_2O_3 crucible. Moreover, reducing the OH groups in TTZ glasses improved the optical properties of Nd^{3+}-doped TTZ glass, and a higher spectral figure of merit of 8.71×10^{-24} s cm^2 for Nd^{3+}:$^4F_{3/2} \rightarrow {}^4I_{11/2}$ emission at 1,075 nm could be achieved, indicating that Nd^{3+}-doped TTZ glass with lower hydroxyl content is promising for laser or active optical applications.

Keywords: Nd^{3+} ions; TeO_2-TiO_2-ZnO glasses; lower hydroxyl content; Judd-Ofelt analysis; glass structure; stimulated emission cross-section

1. Introduction

Rare-earth (RE) ion-doped tellurite glasses have attractive optical properties, including high refractive index (>2.0), wide optical window from near-ultraviolet (NUV) to infrared (IR) region and a variety of photoluminescence (PL), as well as low melting point, good chemical stability and high solubility of RE ions.**[1-8]** Low phonon energy of tellurite glasses (~700 cm^{-1}) is beneficial for obtaining high PL intensity of RE ions doped in a tellurite matrix. However, the residual hydroxyl group (–OH) in the glasses can somewhat influence the optical properties and limit transmission in a

longer-wavelength region, because OH groups strongly absorb IR light at ~ 3,000 cm^{-1}. Such high phonon energy can impair the PL of the RE-ions-doped tellurite glass due to non-radiative transitions known as multiphonon relaxation (MPR).**[9,10]** Recently, we have reported the influence of humidity in glass melt preparation (in open and dry air atmospheres) on the forming ability of tellurite glassy networks, TeO_2-Nb_2O_5-ZnO (TNZ).**[11]** In this case, the incorporation of OH groups could make the glass melt more easily homogenized to form transparent tellurite glasses but was not necessarily favorable for optical applications because of the above mentioned reasons. To reduce OH groups in tellurite glasses, a targeted tellurite system should have a well-developed glassy network and thus, in this study, a TeO_2-TiO_2-ZnO (TTZ) system is adapted, where up to ~10 mol% TiO_2 can be incorporated in the TeO_2 glassy network without changing the Raman spectra.**[12,13]** ZnO is known as an intermediate oxide in glasses and can bridge tellurite networks.**[14,15]** When emissive RE ions are doped in TTZ glass system, ZnO can also play the role of leading more dopant ions, such as Nd^{3+}, into the tellurite glassy network.**[16]** In this study, to obtain TTZ glasses with lower OH contents, highly pure air with low dew point (D.P.) is used and the PL properties of Nd^{3+}-doped TTZ glasses are investigated. Nd^{3+} ions have been widely used for laser applications due to the strong near-infrared (NIR) radiation of $^4F_{3/2} \rightarrow {}^4I_{11/2}$ transition.**[17]**

Influence of crucible used

The structures and optical properties of glasses are influenced by the type of crucible selected in glass preparation and the glass composition adapted. Thus, we also show how the use of different types of crucibles influences the resultant tellurite glass structures. A typical selection would be Al_2O_3, because of cost-effectiveness, which therefore matches to industrial mass production, but special care should be taken to avoid the incorporation of Al_2O_3 with a significant level of contamination.**[11,15,18]** To avoid such a contamination, a Pt crucible may be a good alternative. The first part of this paper shall be devoted to compare the structures of TTZ glasses obtained with Al_2O_3 and Pt crucibles by means of Raman spectroscopy.

Why TTZ

Tellurium di-oxide (TeO_2) acts as a network former of glass structures but it is difficult to obtain a single component of amorphous TeO_2 at a normal quenching speed.**[15,19,20]** Thus, a second component of alkali, alkaline-earth and transition metal oxides like WO_3, TiO_2, Nb_2O_5, Bi_2O_3, ZnO etc is intentionally used to obtain stable tellurite-based glasses.**[21-24]** To obtain a much higher refractive index, compounds such as BaO, PbO and Bi_2O_3 are used.**[25-27]** To extend the glass-forming ability an intermediate oxide of ZnO can also be used. Ghribi et al. **[28]** reported the optical properties of TeO_2-TiO_2-ZnO glasses, including linear refractive index, optical bandgap and third-order nonlinear susceptibility, and discussed the role of the ZnO modifier using Raman spectroscopy

data. The component of ZnO is assumed to extend the glass-forming region even when RE ions are doped to provide PL functionalities. In this study, Nd^{3+} ions are doped in TTZ glasses. The latter part of this paper explains the optical properties of Nd^{3+}-doped TTZ glasses synthesized in ambient and dry air atmospheres, where the Judd-Ofelt (JO) analysis is conducted to theoretically predict the optical properties and laser performances of Nd^{3+}-doped TTZ glasses. Conclusively, it is revealed that the efforts of reducing the OH groups in TTZ glasses improved the optical properties of Nd^{3+}-doped TTZ glass, and allowed a higher spectral figure of merit of 8.71×10^{-24} s cm^2 for Nd^{3+}:$^4F_{3/2} \rightarrow {}^4I_{11/2}$ emission at 1,075 nm, indicating that Nd^{3+}-doped TTZ glass with lower hydroxyl content is promising as a laser material.

2. Experimental

2-1. Glass synthesis using different crucibles (Al_2O_3 and Pt)

The composition of zinc-titanium tellurite (TTZ) glass is 85TeO_2-5TiO_2-10ZnO in mol%. TiO_2 and ZnO were purchased from Nacalai Tesque Inc.. and Kishida Chemical Co., respectively, and used as received. TeO_2 was obtained by thermal decomposition of telluric acid (purchased from Aldrich Co.) heated at 550 °C for 10 h. The mixture of TeO_2, TiO_2 and ZnO was melted in two different crucibles, SSA-H grade Al_2O_3 (Nikkato Co.; 95%Al_2O_3-3%SiO_2, 3.7g/cm^3(bulk density)) and Pt. TeO_2, TiO_2 and ZnO were precisely weighted, mixed well, and melted at 950 °C for 30 min or 5 h with intermittent shaking, and quenched on a warm brass mold preheated at ~100 °C. After appropriate annealing at a temperature 50 °C lower than the glass transition temperature (T_g) for 12 h to release surface stress, the resultant glasses were polished to be planar with ~ 1 mm thickness with optical flatness. The optical bandgap was estimated using a UV-Vis-NIR spectrometer (JASCO, UV-670). Tauc plots of the UV-Vis-NIR spectra were drawn to determine the optical bandgap ${E_g}^{opt}$ of the obtained tellurite glasses.**[29-31]**

$$\alpha h\nu = B\left(h\nu - {E_g}^{opt}\right)^p, \quad (1)$$

where α is optical absorption coefficient in cm^{-1}, B is a constant, $h\nu$ is photon energy in eV, and p has values of 1/2, 2, 3/2 and 3 for direct, indirect, forbidden direct, and forbidden indirect transition between the valence and conduction bands, respectively. Here an indirect transition of $p = 2$ is assumed because of no PL under excitation over the optical bandgap energy for non-doped TTZ glasses. From a cross point of two tangential lines in the Tauc plot, the optical bandgap energy ${E_g}^{opt}$ was estimated. The linear refractive index was analyzed by an ellipsometer (FiveLab., MARY-102) using a He-Ne laser (632.8nm). The density was measured by Archimedes method. The thermal properties (T_g, on-set crystallization temperature (T_x), crystallization temperature (T_c), melting point (T_m), and thermal stability $\Delta T\left(= T_x - T_g\right)$) were examined by differential thermal analysis-thermogravimetry (DTA-TG; RIGAKU, TGD9600). The Hruby factor, defined as **[32]**

$$H_r = \frac{T_x - T_g}{T_m - T_x} \quad (2)$$

is also calculated. Raman spectra were measured by a Raman spectrophotometer (JASCO, NRS-2000) using a diode-pumped solid-state laser at 532 nm with 10 mW power. The obtained Raman spectra were deconvoluted with Gaussian functions to evaluate the percentages of tellurite unit structures (trigonal bipyramids (TeO_4), intermediate (TeO_{3+1}) and trigonal pyramid (TeO_3)) **[33-36]** which are related to the glass structure of zinc-titanium tellurite glasses (**Fig.1**). An elementary analysis for the obtained TTZ glasses was conducted using the X-ray fluorescence (XRF) method (SII, SEA2200A). NIR PL experiments were conducted under 808 nm excitation of a diode laser (JDS Uniphase, SDL-2362).

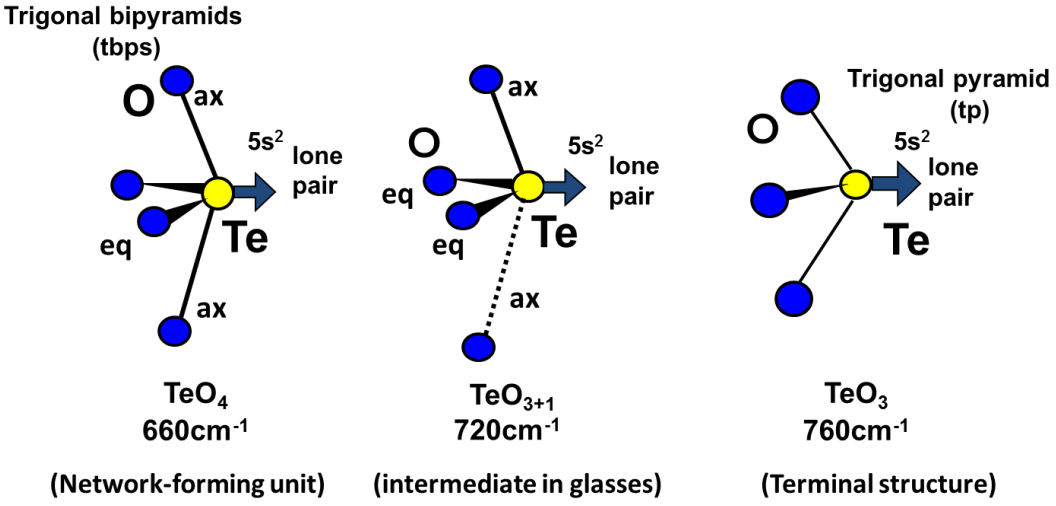

Fig.1 Structural units of tellurite glasses: trigonal bipyramids (tbps) denoted by TeO_4; intermediate, denoted by TeO_{3+1}; and terminal trigonal pyramid (tp) with a double bond Te=O, denoted by TeO_3, which are detectable in Raman spectroscopy.

2-2. Attempt to synthesize TTZ glasses with low hydroxyl groups

Nd_2O_3 (0.5wt%; Kojyundo Kagaku Co.) was doped in $85TeO_2$-$5TiO_2$-10ZnO glass. The glass melts were prepared in two different atmospheres; ambient air and dry air with grade "G2" (D.P.< -60 °C, $CO(CO_2)$ < 0.5ppm, $NO_x(SO_2)$ < 0.05ppm). A Pt crucible was used for Nd^{3+}-doped TTZ glasses. In ambient atmosphere, the glass melt, maintained for 30 min. at 950 °C with intermittent shaking, was casted in the same way as the case of the non-doped TTZ glasses. In dry atmosphere synthesis, a mixture of TTZ and Nd_2O_3 was preheated at 200 °C for 12 h, and subsequently heated at 950 °C for 30 min and cooled down in a tube furnace through which the "G2"-grade dry air was passing continuously. The moderately cooled glass in the Pt crucible was transferred in a grove box filled with "G2"-grade dry air and again heated in a box-type furnace at 950 °C for 5 min. to be casted on a warm

brass mold at 100 °C after being shaken several times. The obtained glass was characterized using a Fourier transform-Infrared (FT-IR) spectrometer (JASCO, FT/IR-410) to estimate the residual OH contents. These procedures were repeated four times. Finally the glass was annealed in the same way as the non-doped TTZ glasses but in the dry air atmosphere. The glasses obtained were polished to 2 mm thickness for further optical measurements. All experiments were conducted at room temperature.

2-3. Estimation of OH amounts in glasses

The amount of hydroxyl groups N_{OH} in unit volume was estimated using the OH vibration band at around 3,000 cm^{-1} in FT-IR spectra.**[37,38]**

$$N_{OH} = \frac{N_A}{\varepsilon_{OH} L} ln\left(\frac{1}{T}\right), \quad (3)$$

where N_A is the Avogadro constant, ε_{OH} is the molar absorption coefficient of OH groups (49.1 dm^3 mol^{-1} cm^{-1}), L is the sample thickness in cm, and T is IR transmittance. The OH content in glass is given by

$$C_{OH} = \frac{N_{OH} W_{OH}}{N_{OH} W_{OH} + N_{Glass} W_{Glass}} \quad (4)$$

(N_{Glass} is the amount of glass in unit volume, and W_{OH} and W_{Glass} are the molar weight of OH and glass, respectively.)**[39]**

2-4. JO analysis of optical properties of Nd^{3+} in glasses

We briefly explain the JO analysis **[40-42]** of Nd^{3+}-doped TTZ glasses. The optical absorption spectra from visible to IR region were taken as molar absorbance ε (dm^3 mol^{-1} cm^{-1}) for Nd^{3+} as a function of wavenumber ν of the incident photon in cm^{-1}, $\varepsilon(\nu) = \mathrm{OD}(\nu)/C_{Nd}L$, where $\mathrm{OD}(\nu)$ is the optical density as function of ν, C_{Nd} is the Nd molar concentration in mol/dm^3, and L is the sample thickness in cm. The absorption peaks due to f-f transition of the doped Nd^{3+} were estimated to obtain the integrated band intensity and oscillator strength f_{exp} as follows.

$$f_{exp} = 4.318 \times 10^{-9} \int \varepsilon(\nu)\, d\nu \quad (5)$$

The absorption intensity of f-f transition is regarded as a sum of two contributions: electric and magnetic dipole transitions, $f_{exp} = f_{ed} + f_{md}$, which are respectively expressed as

$$f_{ed} = \frac{8\pi^2 mc\nu}{3h(2J+1)} \left(\frac{(n^2+2)^2}{9}\right) S_{ed} \quad (6)$$

$$f_{md} = \frac{8\pi^2 mc\nu}{3h(2J+1)} n S_{md} \quad (7)$$

where ν is the wavenumber of energy between the levels denoted by J and J' manifolds corresponding to the initial and final state of transitions, respectively; m is the mass of an electron; n is the refractive index; c is light velocity; and h is the Planck's constant. S_{ed} and S_{md} indicate the

line strength for electric and magnetic dipole transitions, respectively. In general, the contribution of magnetic dipole transition to absorption intensity is negligible. Even if not, S_{md} is only dependent on the refractive index and thus the contribution is theoretically calculated, which can be referred to from Carnall et al.**[43]**

The electric dipole line strength S_{ed} can be expressed with three individual parameters, called Ω parameters (or JO parameters), $\Omega_{2,4,6}$.

$$S_{ed} = e^2 \sum_{t=2,4,6} \Omega_t \, |\langle (S,L)J||U^t||(S',L')J'\rangle|^2 \ , \quad (8)$$

where $|\langle (S,L)J||U^t||(S',L')J'\rangle|$ is a *t*-th ranked tensor for a transition from levels $(S,L)J$ to $(S',L')J'$, whose tables are available in the literatures.**[44,45]** Substantially, $\Omega_{2,4,6}$ are phenomelogical parameters that well-characterize the optical properties due to f-f transition of RE ions doped in materials. The parameters can be calculated using the Gauss-Seidel algorithm from the S_{ed} values of eight different absorption bands experimentally obtained for Nd^{3+}-doped TTZ glasses, $^4I_{9/2}$ → $^4I_{13/2}$, $^4_{15/2}$, $^4F_{3/2}$, $^4F_{5/2}$+$^2H_{9/2}$, $^4F_{7/2}$+$^4S_{3/2}$, $^4F_{9/2}$, $^4G_{5/2}$+$^2G_{7/2}$, and $^2K_{13/2}$+$^4G_{7/2}$+$^4G_{9/2}$. The accuracy of the estimation is observed as a root mean square (RMS) deviation for oscillator strength, as follows.**[44]**

$$\delta_{RMS} = \frac{(\text{sum of squares of deviation})^{\frac{1}{2}}}{(\text{No.of transitions} - \text{No.of parameters})^{\frac{1}{2}}} \ , \quad (9)$$

which is also used to obtain RMS error % defined as a ratio of δ_{RMS} against averaged $\bar{f}_{exp}$ obtained from squares of experimental oscillator strengths. Once $\Omega_{2,4,6}$ parameters are known, the luminescence properties between two different levels, J and J', can be theoretically predicted as a radiative transition probability, A:

$$A = A_{ed} + A_{md} = \frac{64\pi^4\nu^3}{3h(2J+1)}\left\{\frac{n(n^2+2)^2}{9} S_{ed} + n^3 S_{md}\right\} \quad (10)$$

The former is the contribution of electric dipole transition, while the latter is obtained from magnetic dipole transition, of a spontaneous emission. The emissive level which is an initial state of luminescence, $|i\rangle$, sometime provides several luminescence lines with different final states, denoted by $|j\rangle$. Then a branching ratio $\beta_{i\to j}$ can be defined as

$$\beta_{i\to j} = \frac{A_{i\to j}}{\sum_j A_{i\to j}} \quad (11)$$

and the radiative lifetime can be theoretically determined by the following equation.

$$\tau_i = \left(\sum_j A_{i\to j}\right)^{-1} \quad (12)$$

The stimulated emission cross section σ_{em} is given by the Fuchtbauer-Ladenburg (FL) equation: **[46,47]**

$$\sigma_{em} = \frac{{\lambda_p}^4}{8\pi c n^2 \Delta\lambda} A_{i\to j} \ , \quad (13)$$

where $A_{i\to j}$, λ_p and $\Delta\lambda$ indicate the radiative transition probability, peak wavelength and effective

linewidth, respectively, of the laser emission line, in case of Nd^{3+}, $^4F_{3/2}$-$^4I_{11/2}$ transition around 1,060 nm,

$$\lambda_p = \frac{\int \lambda\, I(\lambda)\, d\lambda}{\int I(\lambda)\, d\lambda} \quad (14)$$

$$\Delta\lambda = \frac{\int I(\lambda)\, d\lambda}{I_{max}}. \quad (15)$$

2-5. Theoretical prediction of laser performance for Nd^{3+}-doped tellurite glasses

The spectroscopic figure of merit (FOM) can be introduced to predict the likelihood in a low-threshold operation. A large FOM value implies a low laser threshold of the laser host. FOM can be expressed as **[48]**

$$\text{FOM} = \sigma_{em}\tau_{eff}\ , \quad (16)$$

where τ_{eff} is the experimental lifetime.

In general, the laser performance of a material can be predicted theoretically by calculating the absorption and emission cross section by using the Beer-Lambert equation and McCumber (MC) theory, given as**[49]**

$$\sigma_{abs}(\lambda) = \frac{2.303\ OD(\lambda)}{C_{Nd}L} \quad (17)$$

$$\sigma_{em}^{MC}(\lambda) = \sigma_{abs}(\lambda)\frac{Z_L}{Z_U} exp\left\{\frac{hc}{k_BT}\left(\frac{1}{\lambda_{ZL}} - \frac{1}{\lambda}\right)\right\}, \quad (18)$$

where σ_{abs} is the absorption cross section, σ_{em} is the stimulated emission cross-section, Z_L/Z_U is the population function of the lower ($^4I_{11/2}$) and upper ($^4F_{3/2}$) levels tested at a low temperature or can be approximately replaced by the ratio of degeneracy of the upper and lower energy levels at high temperature, k_B is the Boltzmann constant, T is the temperature in Kelvin, and λ_{ZL} = 1,081 nm is the zero phonon line.

The gain function is also one of the important parameters for RE-doped laser materials. If the Nd^{3+} ions are only distributed at the $^4F_{3/2}$ and $^4I_{11/2}$ levels, the gain coefficient can be calculated as **[50]**

$$G(\lambda) = N_A C_{Nd}[\xi\sigma_{em}(\lambda) - (1-\xi)\sigma_{abs}(\lambda)], \quad (19)$$

where, $G(\lambda)$ is the gain coefficient from the upper level to the lower level at wavelength λ and ξ is a reversal factor value from 0 to 1, representing the ratio of upper-level populations to the totals.

3. Results

3-1. Influences of different crucible types on fundamental properties of tellurite TTZ glasses

All TTZ glasses obtained in this study are amorphous, as confirmed by X-ray diffraction (XRD). **Table 1** summarizes the density *d*, linear refractive index *n*, optical bandgap energy $E_g{}^{opt}$ and absorption edge wavelength $\lambda_{\text{edge}}^{\text{NUV}} = E_g{}^{opt}/1240$ for TTZ glasses synthesized with different

crucibles (Al_2O_3 and Pt). The main distinguishing factor is that TTZ glass synthesized with Al_2O_3 crucible (TTZ-Al_2O_3) has lower density, as well as lower linear refractive index, than that of the TTZ glass synthesized with Pt crucible (TTZ-Pt). The optical bandgap $E_g{}^{opt}$ of TTZ-Al_2O_3 is higher than that of TTZ-Pt (the respective Tauc plot for determining the gap is depicted in **Fig.2** as inset), clearly evidenced from the fact that TTZ-Al_2O_3 glass is transparent and has no color while TTZ-Pt is slightly yellow-colored. These results indicate that TTZ-Al_2O_3 and TTZ-Pt glasses have substantially different structures despite the same starting composition. The thermal properties of TTZ-Al_2O_3 and TTZ-Pt glasses are also summarized in **Table 1**, where TTZ-Al_2O_3 has higher T_g and thermal stability $\Delta T(= T_x - T_g)$. The Hruby factor is also higher for TTZ-Al_2O_3 glasses, indicating the higher thermal stability of TTZ-Al_2O_3. A comparison of the thermal properties of the two glasses elucidates that the crucible selection considerably influences the thermal behaviors of the resultant glasses.

Table 1. Density *d*, linear refractive index *n*, optical bandgap energy $E_g{}^{opt}$ and absorption edge wavelength $\lambda_{edge}^{NUV}(= 1240/\ E_g{}^{opt})$ in NUV and λ_{edge}^{IR} in IR region (determined by FT-IR spectra), and thermal properties (glass transition temperature (T_g), on-set crystallization temperature (T_x), crystallization temperature (T_c), melting point (T_m), thermal stability $\Delta T(= T_x - T_g)$ and Hruby factor H_r) for TTZ glasses synthesized with different crucibles (Al_2O_3 and Pt)

	d / g cm^{-3}	n	$E_g{}^{opt}$ / eV	λ_{edge}^{NUV} / nm	λ_{edge}^{IR}/ nm	T_g / °C	T_x / °C	T_c / °C	T_m / °C	ΔT / °C	H_r
TTZ-Al_2O_3	4.96	2.01	3.00	415	5,508	384	531	562	642	147	1.83
TTZ-Pt	5.45	2.19	2.88	440	5,878	323	395	423	612	72	0.33

Figure 2 shows optical transmission spectra of TTZ-Al_2O_3 and TTZ-Pt glasses, ranging from UV to IR region. The large absorption band at 3,000 nm is due to OH vibrations. The infrared absorption edge, defined as a wavelength with half the maximum transmission, is found to be different between TTZ-Al_2O_3 (~ 5,500 nm) and TTZ-Pt (~ 5,900 nm), revealing that TTZ-Pt itself has a wider optical window from 440 to 5,900 nm. However, the windows for optical applications as IR devices are quite significantly limited up to ~3,000 nm in both glasses due to strong OH vibrations, which should be reduced for further considerations of tellurite glasses for IR applications. The data of transmission to TTZ-Al_2O_3 have a slope down to a shorter UV from the IR region and in fact TTZ-Al_2O_3 is slightly opaque, which might suggest light scattering by an inclusion.

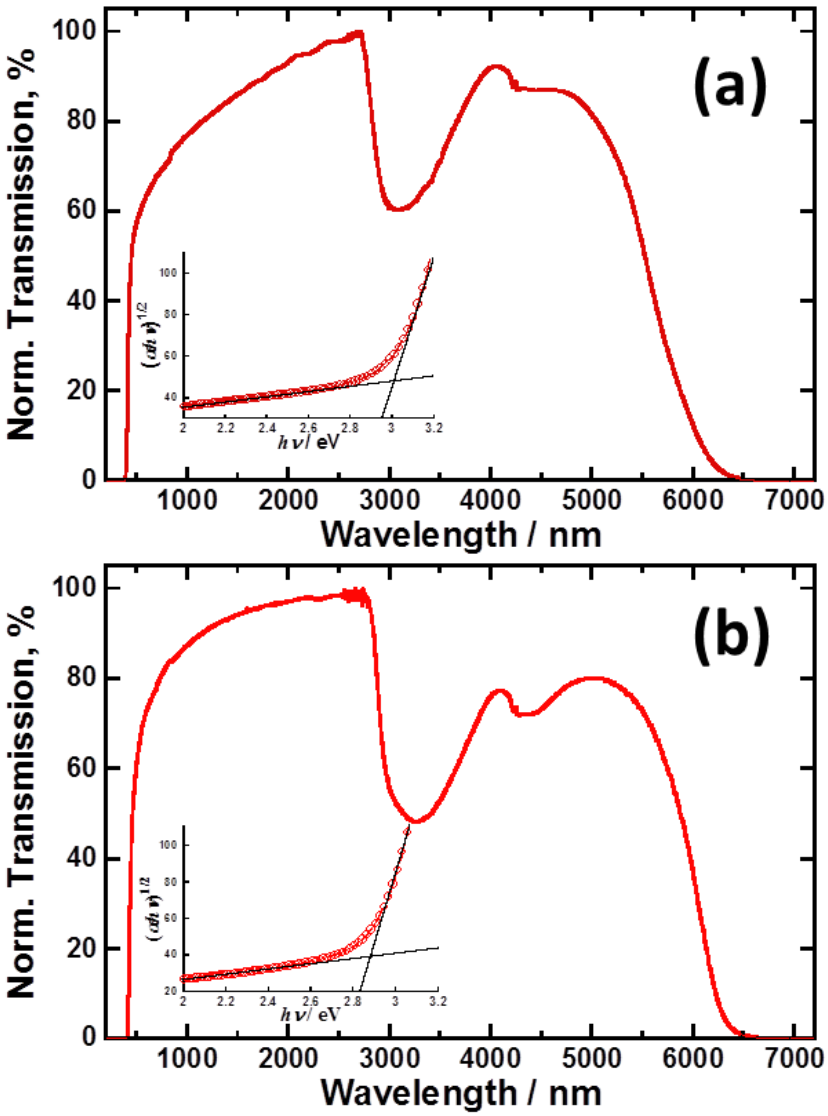

Fig.2 Transmittance of $85TeO_2$-$5TiO_2$-10ZnO glass synthesized with (a) alumina (TTZ-Al_2O_3) and (b) Pt crucible (TTZ-Pt). The insertions show Tauc plots around the NUV absorption edge for the respective glasses.

3-2. XRF and Raman analyses of TTZ glasses synthesized with different crucibles

To elucidate why TTZ-Al_2O_3 and TTZ-Pt glasses have such different properties, as shown in **Table 1**, we perform XRF analysis, whose results are shown in **Table 2**. A prominent difference between the two glasses is found, in that the additional incorporation of Al_2O_3 content to TTZ glass, which would come from the crucible, is detected to be 10~11 wt% (or 14~15 atm% with the Al element) in TTZ-Al_2O_3, while TTZ-Pt has one unit closer than the theoretical composition of $85TeO_2$-$5TiO_2$-10ZnO. However, TeO_2 and ZnO are slightly volatile because of the higher melting temperature of 950 °C.

The XRF analysis cannot detect any Pt components at an appropriate accuracy. In TTZ-Al_2O_3, the volatilization of TeO_2 even for a longer melting time of ~ 5 h is restricted such that Te:Ti:Zn=85.2:6.3:7.1 (calculated without Al_2O_3) against Te:Ti:Zn=78.3:8.78:12.9 for TTZ-Pt(5h), which might be a reason why the TeO_3 terminal structures are dominant in TTZ-Al_2O_3, as later seen in Raman analysis. The incorporation of Al_2O_3 component can stabilize the tellurite glass structure, increasing ΔT and H_r (**Table 1**), which is a positive aspect of Al_2O_3 acting as an intermediate oxide in glass. Nevertheless, as a host material for photoluminescent activator ions, a high refractive index is beneficial, and such Al_2O_3 component obtained from the crucible makes the optical properties of tellurite glasses unreliable. Thus, tellurite glasses for optical applications such as Nd^{3+} lasers should better be synthesized with a Pt crucible, which is adapted in the subsequent part of this paper.

Table 2. Results of elementary analysis by XRF method

XRF	TTZ-Al_2O_3 (30min)	(5h)	TTZ-Pt (30min)	(5h)
Te (atm%)	73.4±0.7	73.4±0.7	83.9±0.7	78.3±0.7
Ti (atm%)	5.8±0.2	5.4±0.2	7.9±0.2	8.8±0.2
Zn (atm%)	6.9±0.1	6.2±0.1	8.2±0.1	12.9±0.1
Al (atm%)	13.9±0.2	15.0±0.2	-	-

To discuss more the differences between TTZ-Al_2O_3 and TTZ-Pt glasses in detail, we perform Raman experiments, whose results are shown in **Fig.3** after base-line correction. As it can be seen, the obtained Raman spectra are quite different. The Raman spectrum of TTZ-Al_2O_3 has a broader feature in a higher-wavenumber region. The deconvoluted data and their assignment are given in **Table 3**. The Raman band located from 340 to 540 cm^{-1} is assigned to Te-O-Te(Ti, Zn) bending vibrations. The stretching vibration of Te-O in TeO_4 tbps, TeO_{3+1} intermediate and terminal TeO_3 tp unit structures are observed at around 580~660, 720 and 750~775 cm^{-1}, respectively. The main difference in Raman bands between TTZ-Al_2O_3 and TTZ-Pt can be found as the increasing fraction of TeO_4 bands for TTZ-Pt and the larger contribution of TeO_3 band for TTZ-Al_2O_3. The fractional numbers of the unit structures are estimated with the respective band area, as tabulated in **Table 3**, which includes the analyzed data for TTZ glasses obtained with a longer melting time of 5 h. For the TTZ-Pt glass, TeO_4 unit structures are dominant in comparison to TeO_3 terminal unit structures, and the intermediate TeO_{3+1} structures are increased when the melt is treated for 5 h, indicating that TiO_2 and ZnO are network-forming for connecting TeO_4 and TeO_{3+1} units, rather than acting as modifiers to be terminated with TeO_3 units. On the other hand, TTZ-Al_2O_3 has more TeO_3 than TeO_4 unit structures, which might be due to contribution of Al-O bonds in Raman spectra. The bending band intensity of

Te-O-Te(Ti,Zn) is considered to be an index to evaluate tellurite's network-connectivity. TTZ-Pt glasses have more Te-O-Te(Ti, Zn) bonds than TTZ-Al_2O_3 regardless of the melting times. According to the XRF data mentioned above, it is clear that the incorporation of Al_2O_3 can change the glass structure of TTZ to have more TeO_3 unit structures and lesser Te-O-Te(Ti, Zn) connectivities. The present spectroscopic data were enough to elucidate the difference in Raman spectra between TTZ-Al_2O_3 and TTZ-Pt glasses, however, unfortunately some crystallization was evidenced. Please bear in mind that the initial glasses were all amorphous. The laser power used here ~10 mW was not too strong but a long exposure time ~10 sec and typically 4 times average to acquire the data might not be too short.

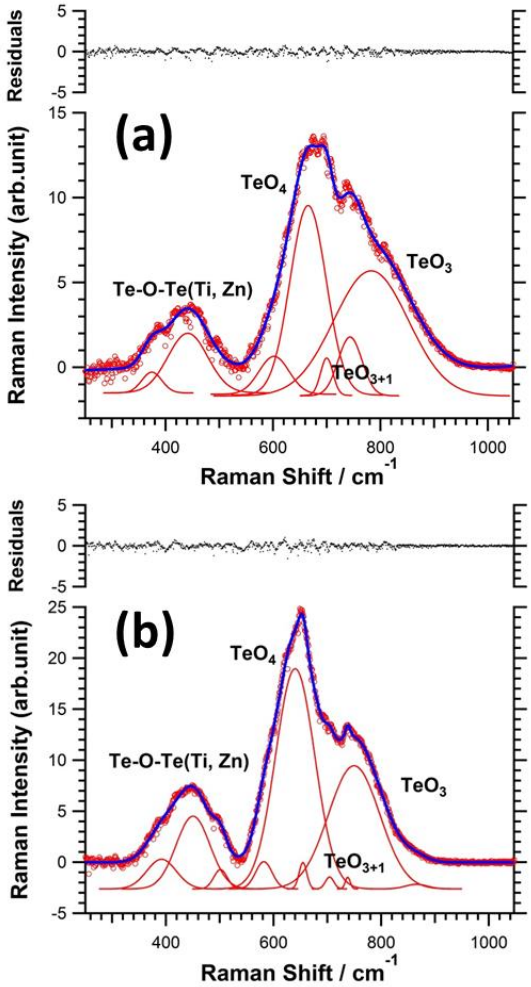

Fig.3 Deconvoluted Raman spectra of 85TeO_2-5TiO_2-10ZnO glasses synthesized with (a) alumina (TTZ-Al_2O_3) and (b) Pt crucible (TTZ-Pt).

Table 3 Ratio of TeO_x unit structures of non-doped TTZ glasses synthesized with different crucibles (Refer also Fig.3).

	TTZ-Al_2O_3 (30min)	(5h)	TTZ-Pt (30min)	(5h)
TeO_4, 580~660 cm^{-1}	41.8	39.1	58.6	45.9
TeO_{3+1}, ~720 cm^{-1}	9.6	8.0	0.6	13.3
TeO_3, 750~775 cm^{-1}	48.6	52.9	40.8	40.8
Te-O-Te(Ti, Zn), 340~540 cm^{-1}	14.6	12.6	22.6	20.6

3-3. OH content in Nd^{3+}-doped TTZ glasses

To derive out reasonable performance of photonic glasses for lasers, optical sensors, and nonlinear optical devices, glass synthesis of well-designed glass compositions like TTZ glasses in a controlled manner is indispensable. The influence of the crucible used is significant, as shown in the proceeding section (**3-1** to **-2**), and is found to largely change the glass structure. Here we use a Pt crucible for preparing $85TeO_2$-$5TiO_2$-10ZnO glass doped with Nd^{3+} ions. The hydroxyl groups are to be still incorporated in glasses as an impurity. For the purpose to reduce OH content, low humidity atmosphere is used in the glass melt preparation, where OH groups also have significant influences on the homogeneity of the glass melts, as discussed in our previous paper on the TeO_2-Nb_2O_5-ZnO system, so that the transparency of the tellurite glasses obtained was substantially. As for TTZ glasses, special attention must be paid, as well. Additionally, to avoid any crystallization during laser experiments as seen in Raman data, rapid quenching and sufficient annealing around at T_g were carefully conducted. This section shows the amount of OH contents lowered in TTZ glasses and discusses the Judd-Ofelt analytical data for Nd^{3+}-doped TTZ glasses synthesized in ambient and dry atmospheres, which are denoted by TTZ-A and TTZ-D, respectively.

The OH contents in Nd^{3+}-doped TTZ glasses are estimated by FT-IR. **Figure 4** show the IR optical transmittance for Nd^{3+}-doped TTZ glasses. The optical absorption of OH vibration bands at ~3,000cm^{-1} is decreased by repeated melting and quenching in dry air atmosphere (D.P. is $-20\sim-10$ °C when the furnace is used) and OH contents are finally reduced to 89.1 ppm (TTZ-D), while melt-quenching in ambient air atmosphere (TTZ-A) results in the OH content of 163.4 ppm (**Fig.5** and **Table 4**). The Nd^{3+}-doped TTZ glass (TTZ-A) has a refractive index of 2.18 which is comparable to that of the non-doped TTZ glass (TTZ-Pt) (**Table 1**). In addition, the TTZ-D glass has n = 2.13, which is slightly lowered by the casting after 5 min of re-melting in the dry atmosphere. This means that some volatile components of TeO_2 and ZnO loosen with OH contents although they are not at a significant level because of the shorter re-melting time. Note that, despite the four rounds of melting and quenching in the dry atmosphere, the OH groups still have residue. One of the reasons for this is the use of telluric acid as a starting material, $Te(OH)_6 \rightarrow TeO_2 + 3H_2O + 1/2\ O_2$.**[51]** Although it is decomposed to α-TeO_2, confirmed by XRD (not shown here), it is assumed that the hydroxyl groups are chemically

adsorbed to prevent their complete removal. Here, none of the fluoride and chloride compounds for starting chemicals, such as ZnF and ZnCl, are used, to avoid the generation of HF and HCl in a nearly closed system when casting. However, the reduced OH contents can somewhat impact the optical properties of Nd^{3+}-doped TTZ glass, as shown in the subsequent section.

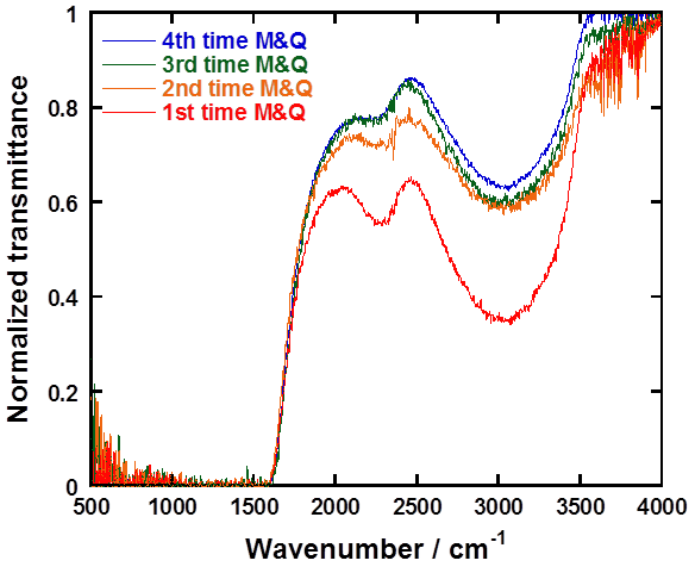

Fig.4 Normalized transmittance of Nd^{3+}-doped TTZ glasses synthesized with Pt crucible in dry atmosphere (D.P. :-20 to -10°C) by repeated melting and quenching (M&Q) in a grove box.

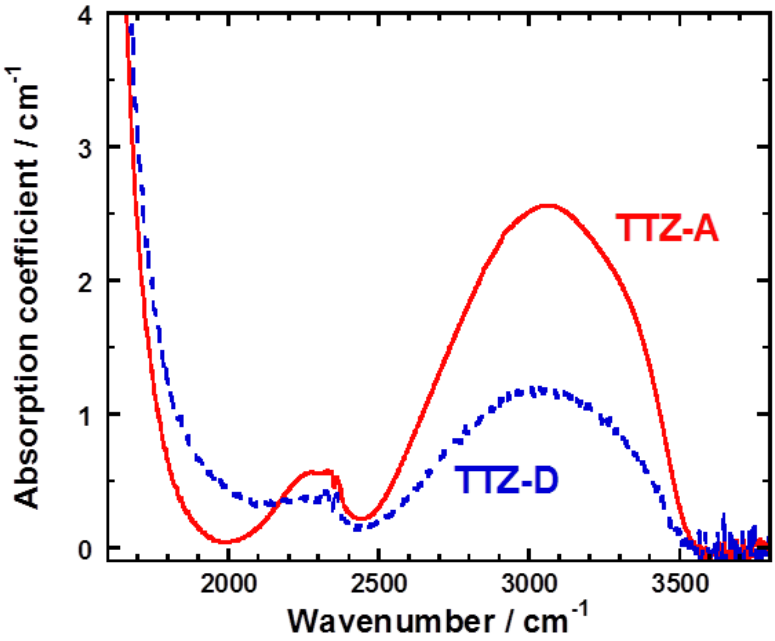

Fig.5 Absorption coefficient of Nd^{3+}-doped TTZ glasses synthesized in ambient atmosphere (TTZ-A) and in dry atmosphere (D.P. -20 to -10 °C) in a grove box (4times re-melting and quenching) (TTZ-D).

3-4. Optical properties of Nd^{3+} ions in TTZ glasses synthesized in ambient and dry air atmosphere

Figure 6 shows the UV-Vis absorption spectra of Nd^{3+}-doped TTZ glass. Several absorption bands due to f-f transitions of Nd^{3+} are observed, which are assigned to transitions from the ground state $^4I_{9/2}$ to excited states: $^2K_{13/2}+^4G_{7/2}+^4G_{9/2}$ (~520nm), $^4G_{5/2}+^2G_{7/2}$ (~580nm), $^4F_{9/2}$ (~690nm), $^4F_{7/2}+^4S_{3/2}$ (~750nm), $^4F_{5/2}+^2H_{9/2}$(~808nm), $^4F_{3/2}$(~890nm), $^4I_{15/2}$(~1700nm) and $^4I_{13/2}$(~2500nm).**[47]** The band intensities are integrated after Gaussian function fittings to calculate oscillator strengths for the transitions, which are summarized in **Table 4**. The actual Nd^{3+} concentrations of both glasses for estimating the oscillator strengths are determined by XRF and energy-dispersive X-ray spectroscopy (EDS). Note first that the experimental absorption profile and band intensity of $^4I_{9/2}\rightarrow{}^4I_{15/2}$ are quite different between the two glasses (See [ii] in **Fig.6(a) and (b)**). However, the smaller strength on the order of 0.01 to 0.1×10^{6} eventually itself contributes less to the resulting JO parameters. The theoretical oscillator strengths obtained using the JO method are given in the same table and can be compared with the experimental values. The RMS deviation δ_{RMS} (RMS error) is 0.443×10^{-6} (3.8%) and 0.798×10^{-6} (7.2%) for TTZ glasses synthesized in the low hydroxyl and ambient atmospheres, respectively, which guarantee the computation accuracy. The JO parameters are calculated to be $\Omega_2 = 3.94$ pm^2, $\Omega_4 = 4.79$ pm^2, and $\Omega_6 = 3.90$ pm^2 for TTZ-D, and $\Omega_2 =$

4.32 pm^2, $\Omega_4 = 4.02\ pm^2$, and $\Omega_6 = 3.66\ pm^2$ for TTZ-A. The spectroscopic quality factor $\chi = \Omega_4/\Omega_6$ **[48]** can effectively estimate the intrinsic intensities of $^4F_{3/2}\rightarrow{}^4I_{9/2}$ and $^4F_{3/2}\rightarrow{}^4I_{11/2}$ in Nd^{3+}-doped glass. If χ is smaller than 1, the intensity of $^4F_{3/2}\rightarrow{}^4I_{11/2}$ transition will be stronger than that of $^4F_{3/2}\rightarrow{}^4I_{9/2}$ in the glassy matrix, indicating a stronger emission line at 1.06 μm ($^4F_{3/2}\rightarrow{}^4I_{11/2}$ transition).**[52]** We found that the TTZ synthesized in the dry atmosphere has a larger χ value, which affects the theoretical branching ratio observed in **Table 5**.

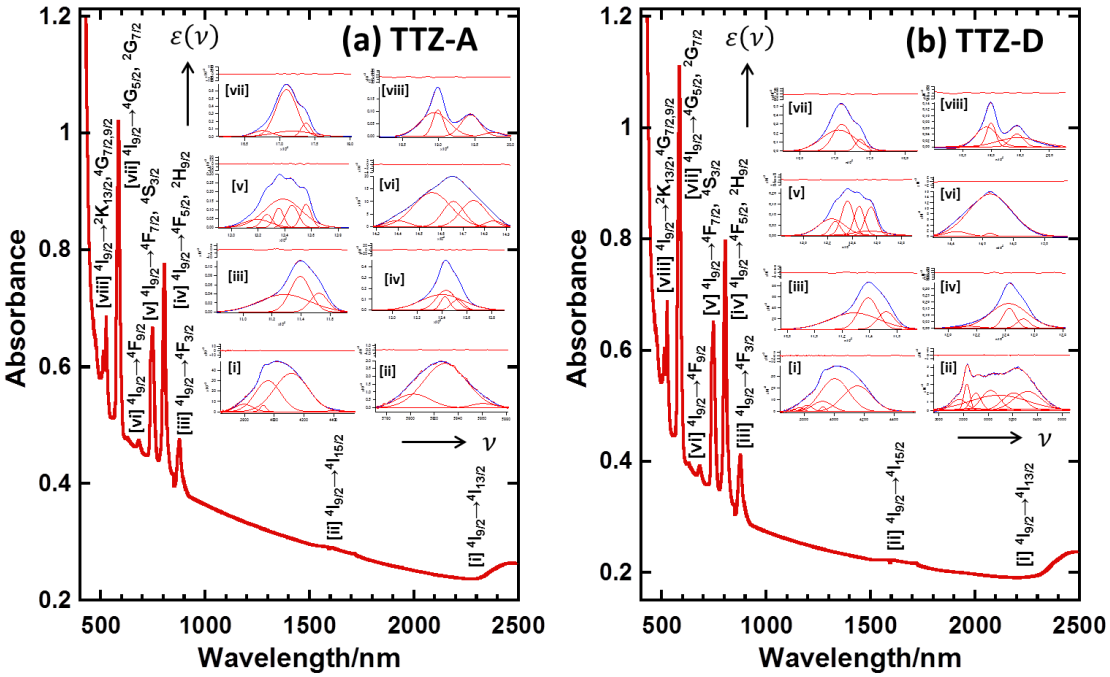

Fig.6 Optical absorption spectra of Nd^{3+}-doped TTZ glasses synthesized in (a) ambient air and (b) dry air atmosphere. The inset shows Nd^{3+} molar absorbance $\varepsilon(\nu)$ as a function of wavenumber in cm^{-1} for transitions from the ground state $^4I_{9/2}$ to excited states: [i] $^4I_{13/2}$ (~2500nm), [ii] $^4I_{15/2}$ (~1700nm), [iii] $^4F_{3/2}$ (~890nm), [iv] $^4F_{5/2}+{}^2H_{9/2}$ (~808nm), [v] $^4F_{7/2}+{}^4S_{3/2}$ (~750nm), [vi] $^4F_{9/2}$ (~690nm), [vii] $^4G_{5/2}+{}^4G_{7/2}$ (~580nm) and [viii] $^2K_{13/2}+{}^4G_{7/2}+{}^4G_{9/2}$ (~520nm), which are deconvoluted with Gaussian functions having smaller residuals between the data and fitting curve to calculate the oscillator strength for each transition.

Table.4 Experimental and calculated oscillator strength values of Nd^{3+}-doped TTZ glass synthesized in ambient and dry air atmospheres.

Transition from $^4I_{9/2}$	Baricenter (cm^{-1})	Ambient air atmosphere TTZ-A n = 2.18 [OH] = 163.4 ppm		Dry air atmosphere TTZ-D n = 2.13 [OH] = 89.1 ppm	
		f_{exp} ($\times 10^6$)	f_{cal} ($\times 10^6$)	f_{exp} ($\times 10^6$)	f_{cal} ($\times 10^6$)
$^4I_{13/2}$	4,036	1.551	1.754	1.588	1.793
$^4I_{15/2}$	5,825	0.015	0.243	0.372	0.248
$^4F_{3/2}$	11,383	3.127	3.226	3.162	3.602
$^4F_{5/2}$, $^2H_{9/2}$	12,434	8.685	9.114	9.700	9.632
$^4F_{7/2}$, $^4S_{3/2}$	13,391	9.525	8.782	9.360	9.016
$^4F_{9/2}$	14,660	0.859	0.716	0.616	0.743
$^4G_{5/2}$, $^2G_{7/2}$	17,106	29.48	29.51	28.59	28.64
$^2K_{13/2}$, $^4G_{7/2}$, $^4G_{9/2}$	18,961	10.02	7.842	9.004	8.236
δ_{RMS} ($\times 10^{-6}$) (RMS error)		0.798 (7.21%)		0.443 (3.79 %)	
Ω_2 / pm^2		4.32		3.94	
Ω_4 / pm^2		4.02		4.79	
Ω_6 / pm^2		3.66		3.90	
$\chi = \Omega_4/\Omega_6$		1.10		1.23	

Figure 7 shows the NIR PL spectra excited at 808 nm. Three strong three PL lines are detected around 900, 1070, and 1340 nm,**[53]** which are attributed to $^4F_{3/2} \rightarrow {}^4I_{9/2}$, $^4I_{11/2}$ and $^4I_{13/2}$ transitions, respectively, all of which agree with those calculated from our optical absorption data. The experimental branching ratios β of $^4F_{3/2}$ to the lower levels are estimated and shown in **Table 5**. The contribution of $^4F_{3/2} \rightarrow {}^4I_{15/2}$ to total emissions from $^4F_{3/2}$ level is found to be < 0.5 % and thus not included in the β values shown. Clearly, TTZ-D glass has a higher branching ratio of 74.9 % for $^4F_{3/2} \rightarrow {}^4I_{11/2}$. Notably, the experimental β value of $^4F/_{3/2} \rightarrow {}^4I_{9/2}$ is quite lower than the theoretical prediction. According to Mann and DeShazer, **[42,54]** the reason for this difference in the line intensities of $^4F_{3/2} \rightarrow {}^4I_{J'}$ (J'=9/2, 11/2, and 13/2) transition can be explained by the "Resonant Fluorescence Trapping (RFT)" of $^4I_{9/2} \rightarrow {}^4F_{3/2}$.

The stimulated emission cross section of $^4F_{3/2} \rightarrow {}^4I_{11/2}$ is given by the radiative transition probability A obtained from the JO analysis and the PL line shape (λ_p, $\Delta\lambda$), which has $\sigma_{em} = 3.93 \times 10^{-20}$ cm^2

and $\sigma_{em} = 3.89 \times 10^{-20}$ cm^2, respectively, for the TTZ glasses synthesized in the low hydroxyl and ambient atmospheres (**Table 6**). Note that the former is, although slightly, higher than the latter. **Table 6** also includes literature data of several tellurite-based glass systems. It can be seen that the NIR emission of $^4F_{3/2} \rightarrow {}^4I_{11/2}$ transition for TTZ-D glass has a band width $\Delta\lambda$ broader and a peak wavelength λ_p longer than those for TTZ-A glass and the other glass systems. λ_p contributes more to σ_{em} through **Eq.(13)**, indicating that the drying process can have a positive effect on Nd^{3+} laser specifications.

The PL decay lifetimes examined at 808 nm excitation are 221.4 and 212.8 μs for TTZ glasses synthesized in the low hydroxyl and ambient atmospheres, respectively (**Fig.7**). The spectroscopic FOM for TTZ synthesized in the dry atmosphere is 8.71×10^{-24} s cm^2, which is greater than the values reported in the literatures (**Table 6**).

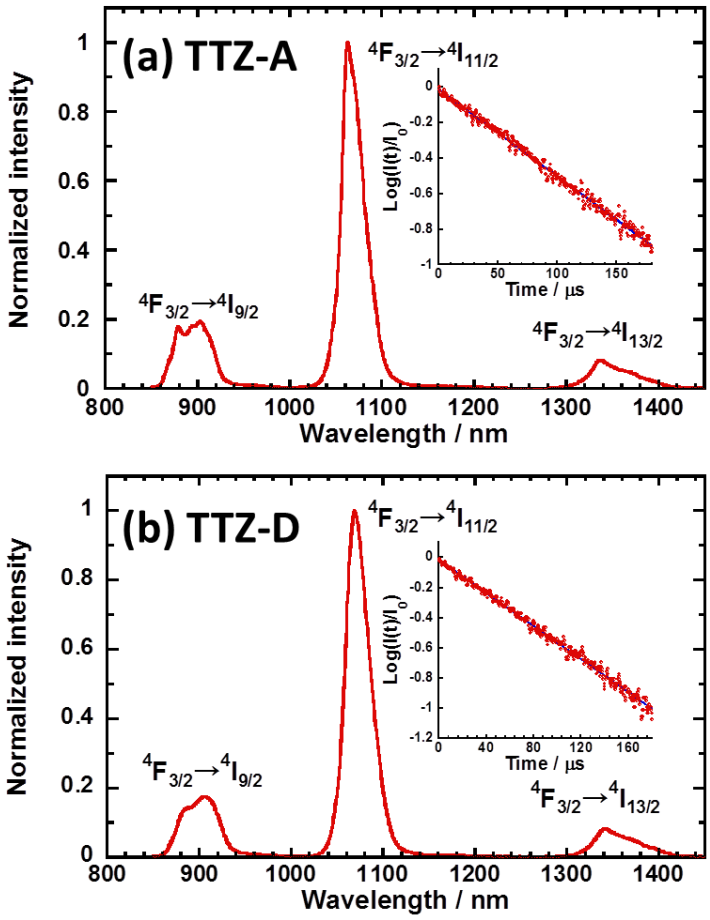

Fig.7 PL spectra and $^4F_{3/2}$ PL decay curves of Nd^{3+}-doped TTZ glass synthesized in (a) ambient air and (b) dry atmosphere(D.P.-20 to -10 °C) in a grove box (4 times melting).

Table.5 Experimental and calculated branching ratio β ($^4F_{3/2} \rightarrow {}^4I_{15/2}$ is neglected

because of its small contribution (< 0.5%)) of Nd^{3+}-doped TTZ glass synthesized in ambient and dry air atmosphere (D.P.-20 to -10°C) in a grove box (4times melting)

Transition process	Ambient air atmosphere TTZ-A		Dry air atmosphere TTZ-D	
	β_{exp} (%)	β_{cal} (%)	β_{exp} (%)	β_{cal} (%)
$^4F_{3/2}\rightarrow{}^4I_{9/2}$	20.6	44.8	19.4	46.4
$^4F_{3/2}\rightarrow{}^4I_{11/2}$	69.6	46.7	74.9	45.6
$^4F_{3/2}\rightarrow{}^4I_{13/2}$	9.8	8.5	5.7	8.0

4. Discussion

The obtained JO parameters for TTZ-A and TTZ-D glasses are all comparable to those reported in the literatures for other Nd^{3+}-doped tellurite glasses; for example, $\Omega_2 = 3.09\ \text{pm}^2$, $\Omega_4 = 3.11\ \text{pm}^2$, and $\Omega_6 = 3.25\ \text{pm}^2$ for Nd^{3+}-doped $85TeO_2$-15ZnO glass (in wt%),**[53]** and $\Omega_2 = 3.11\ \text{pm}^2$, $\Omega_4 = 5.00\ \text{pm}^2$, and $\Omega_6 = 3.87\ \text{pm}^2$ for Nd^{3+}-doped $74.6TeO_2$-8.8ZnO-16.6ZnF_2 glass (in mol%).**[55]** Thus, the calculated radiative lifetimes (τ_{cal} = 135 μs (TTZ-A) and τ_{cal} = 132 μs (TTZ-D)) are also comparative with some reported values: τ_{cal} = 145 μs for TeO_2-ZnO-ZnF systems **[55]** and τ_{cal} = 158 μs for TeO_2-TiO_2-Nb_2O_5 glass.**[56]** Nevertheless, the experimental lifetime for $^4F_{3/2}$ emission is larger than the theoretical prediction. The doping level is 0.5wt% so that Nd^{3+} ions would be free from ion-ion interactions; it is supposed that the Nd^{3+} are isolated well in the TeO_2-TiO_2-ZnO glassy matrix. One of the causes for this is attributed to the strong RFT of $^4I_{9/2}\rightarrow{}^4F_{3/2}$, yielding a lower experimental branching ratio of $^4F_{3/2}\rightarrow{}^4I_{9/2}$ emission shown in **Table 5**. The RFT process can lead to a higher population of $^4F_{3/2}$ level during the emission, and eventually the longer lifetime observed in **Fig.7**.

The FOM value obtained for TTZ-D glass is shown with literature data in **Table 6**, and is found to be higher than the reported ones, due to the relatively longer radiative lifetime and increased radiative emission cross section, σ_{em}. The laser performance can be estimated from **Eqs.(17-19)**. However, since $^4F_{3/2}\rightarrow{}^4I_{11/2}$ of Nd^{3+} is not a transition from an excited state to a ground state, the absorption cross section cannot be estimated from the absorption spectrum. Thus, the "reciprocal method" is used to calculate the absorption cross section of the excited state $^4I_{11/2}$ to $^4F_{3/2}$ level. The result is $\sigma_{abs} = 1.68 \times 10^{-20}\ \text{cm}^2$. **Figure 8(a)** depicts the gain coefficient of $^4F_{3/2}\rightarrow{}^4I_{11/2}$ transition for the Nd^{3+}-doped TTZ glass as a function of reversal factor ξ. The output performance of lasing action can be utilized when $\xi > 0.3$, predicting that this glass has a lower laser threshold than the recently reported case ($\xi > 0.4$) of TeO_2-MoO_3-ZnO.**[48]**

As mentioned about the experimental branching ratio (**Table 5**), the RFT process can eventually repopulate $^4F_{3/2}$ level to increase the reversal factor as an additional process, which is attributed to the strong absorption of $^4I_{9/2}\rightarrow{}^4F_{3/2}$ resulting from the larger contribution of $|\langle|U^4|\rangle|^2 = 0.2293$ **[44]** and

$\chi(=\Omega_4/\Omega_6) = 1.23$. The reduced OH content must minimize the MPR process from $^4F_{3/2}$ to lower levels. Thus, these two processes of the RFT and minimized MPR can increase the population of $^4F_{3/2}$, as schematically illustrated in **Fig.8(b)**. In this study Nd^{3+} ions are pumped via $^4F_{5/2}$ and $^2H_{9/2}$ levels at 808 nm by focused laser excitation and went down to the emissive level of $^4F_{3/2}$. Photoluminescence from $^4F_{3/2}$ to $^4I_{9/2}$ (ground state) and $^4I_{11/2}$, $^4I_{13/2}$ etc can depolulate $^4F_{3/2}$ level. However, the excited state absorption from $^4I_{11/2}$ to $^4F_{3/2}$ ($\sigma_{abs} = 1.68 \times 10^{-20}$ cm^2), larger than that reported in literature **[48]**, can re-polulate $^4F_{3/2}$, and even RFT from $^4I_{9/2}$ can increase the population, as well. Moreover, an additional merit of the minimized MPR can be received so as to increase the population of $^4F_{3/2}$, leading to lower threshold and higher efficiency of lasing actions. Attempts for developing a procedure to further reduce OH groups in tellurite glasses should be continued to apply them to not only efficient RE-doped laser devices but also novel IR tellecomminication/sensors.

Table.6 Stimulated emission cross section σ_{em}, refractive index *n*, radiative transition probability A($^4F_{3/2}\rightarrow{}^4I_{11/2}$), λ_p and $\Delta\lambda$ of $^4F_{3/2}\rightarrow{}^4I_{11/2}$ transition, $^4F_{3/2}$ experimental lifetime τ_{eff} and FOM of several Nd^{3+}-doped tellurite glasses

Glass system	*n*	A($^4F_{3/2}\rightarrow{}^4I_{11/2}$) / s^{-1}	λ_p / nm	$\Delta\lambda$ / nm	σ_{em} ($\times 10^{20}$) / cm^2	τ_{eff} / μs	FOM ($\times 10^{24}$) / s cm^2	Ref
TTZ-D	2.13	3,452	1,075	34.3	3.93	221.4	8.71	This work
TTZ-A	2.18	3,451	1,069	32.3	3.89	212.8	8.28	This work
TZF[a]	2.06	3,130	1,059	25	4.90	128	6.28	**[55]**
TZ[b]	2.01	2,182	1,062	29.3	3.11	217	6.75	**[53]**
TMZ[c]	2.08	2,659	1063	32.7	3.12	192.7	6.02	**[48]**
TTN[d]	2.19	2,920	1076	27.8	3.89	146	5.68	**[56]**
TW[e]	~2	2,180	1065	29	3.21	149	4.78	**[57]**
TZN[f]	2	3,135	1061	30.9	4.27	104	4.44	**[58]**
TWY[g]	2.05	2,042	1061	30.4	2.70	150.3	4.06	**[47]**

[a] TZF: 74.6TeO_2-8.8ZnO-16.6ZnF_2(in mol%)/1wt%NdF_3, [b]TZ: 85TeO_2-15ZnO(in wt%)/1wt%Nd_2O_3, [c]TMZ: 70TeO_2-20MoO_3-10ZnO(in mol%)/0.7mol%Nd_2O_3, [d]TTN: 85TeO_2-5TiO_2-15Nb_2O_5(in mol%)/1wt%Nd_2O_3, [e]TW: 80TeO_2-20WO_3 (in mol%)/1.0mol%Nd_2O_3, [f]TZN: 60TeO_2-39ZnO-1Nd_2O_3, [g]TWY: 80TeO_2-15WO_3-4.5Y_2O_3-0.5Nd_2O_3 (in mol%)

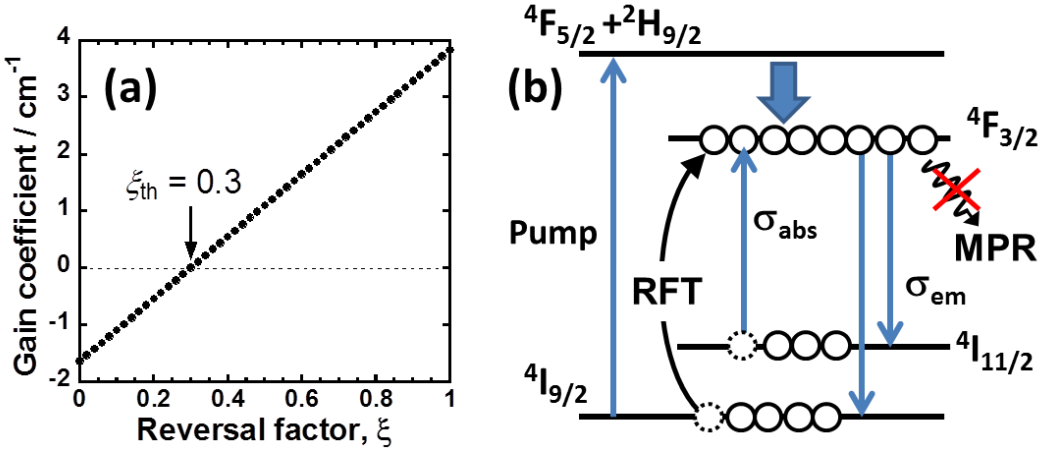

Fig.8 (a) Gain cross section of $^4F_{3/2}$→$^4I_{11/2}$ transition as a function of reversal factor ξ, and (b) schematical illustration of optical transition of $^4F_{3/2}$ emission for lower hydroxyl Nd^{3+}-doped TTZ glass (TTZ-D).

5. Conclusion

In this study, a Nd^{3+}-doped TTZ glass with lower OH groups (down to 89 ppm) was synthesized with Pt crucible. In the first part of the paper, the influence of the use of different crucibles (Al_2O_3 and Pt) on the properties and structures of non-doped TTZ glasses were elucidated. The use of Al_2O_3 crucible caused a contamination of 10-11 wt% level in Al_2O_3, as detected in the resultant TTZ glass (TTZ-Al_2O_3) and restricted the volatilization of TeO_2 and ZnO. However, the incorporation significantly changed the TTZ glass structures, as clarified by Raman spectroscopy. On the other hand, the use of Pt crucible for TTZ glass synthesis (TTZ-Pt) showed more enhancement of the TeO_4 network-forming structure and achieved a higher refractive index of 2.18-9. The JO analysis was performed with an RMS error of 3.8% for Nd^{3+}-doped TTZ-Pt glasses with attempts to reduce the OH groups in the glasses, revealing a higher $\chi = \Omega_4/\Omega_6$ value for Nd^{3+}-doped TTZ glasses. The stimulated emission cross section σ_{em} of $^4F_{3/2}$→$^4I_{11/2}$ was 3.93×10^{-20} cm^2. The longer $^4F_{3/2}$ PL lifetimes were observed for the TTZ glasses, and the obtained FOM was at most 8.71×10^{-24} s cm^2. The decrease in OH contents positively influenced the observed optical properties of Nd^{3+} in TTZ glasses due to an increase in the population of $^4F_{3/2}$ by the RFT and minimized MPR, expecting an efficient laser action of lower hydroxyl Nd^{3+}-doped TTZ glass and a widened optical window up to ~6,000 nm potentially available as IR resources.

Acknowledgements

This research was conducted as a collaborative work of International Scientific Collaboration Project (PICS) between CNRS-IRCER laboratory and Nagoya Institute of Technology (NITech) and in the oversea students exchange program between NITech and Limoges Univ.(ENSIL-ENSCI).

Figure Caption

Fig.1 Structural units of tellurite glasses: trigonal bipyramids (tbps) denoted by TeO_4; intermediate, denoted by TeO_{3+1}; and terminal trigonal pyramid (tp) with a double bond Te=O, denoted by TeO_3, which are detectable in Raman spectroscopy.

Fig.2 Transmittance of $85TeO_2$-$5TiO_2$-10ZnO glass synthesized with (a) alumina (TTZ-Al_2O_3) and (b) Pt crucible (TTZ-Pt). The insertions show Tauc plots around the NUV absorption edge for the respective glasses.

Fig.3 Deconvoluted Raman spectra of $85TeO_2$-$5TiO_2$-10ZnO glasses synthesized with (a) alumina (TTZ-Al_2O_3) and (b) Pt crucible (TTZ-Pt).

Fig.4 Normalized transmittance of Nd^{3+}-doped TTZ glasses synthesized with Pt crucible in dry atmosphere (D.P. :-20 to -10°C) by repeated melting and quenching (M&Q) in a grove box.

Fig.5 Absorption coefficient of Nd^{3+}-doped TTZ glasses synthesized in ambient atmosphere (TTZ-A) and in dry atmosphere (D.P. -20 to -10 °C) in a grove box (4times re-melting and quenching) (TTZ-D).

Fig.6 Optical absorption spectra of Nd^{3+}-doped TTZ glasses synthesized in (a) ambient air and (b) dry air atmosphere. The inset shows Nd^{3+} molar absorbance $\varepsilon(\nu)$ as a function of wavenumber in cm^{-1} for transitions from the ground state $^4I_{9/2}$ to excited states: [i] $^4I_{13/2}$ (~2500nm), [ii] $^4I_{15/2}$ (~1700nm), [iii] $^4F_{3/2}$ (~890nm), [iv] $^4F_{5/2}$+$^2H_{9/2}$ (~808nm), [v] $^4F_{7/2}$+$^4S_{3/2}$ (~750nm), [vi] $^4F_{9/2}$ (~690nm), [vii] $^4G_{5/2}$+$^4G_{7/2}$ (~580nm) and [viii] $^2K_{13/2}$+$^4G_{7/2}$+$^4G_{9/2}$ (~520nm), which are deconvoluted with Gaussian functions having smaller residuals between the data and fitting curve to calculate the oscillator strength for each transition.

Fig.7 PL spectra and $^4F_{3/2}$ PL decay curves of Nd^{3+}-doped TTZ glass synthesized in (a) ambient air and (b) dry atmosphere(D.P.-20 to -10 °C) in a grove box (4 times melting).

Fig.8 (a) Gain cross section of $^4F_{3/2}\rightarrow{}^4I_{11/2}$ transition as a function of reversal factor ξ, and (b) schematical illustration of optical transition of $^4F_{3/2}$ emission for lower hydroxyl Nd^{3+}-doped TTZ glass (TTZ-D).

References

[1] R.A.H.El-Mallawany, Tellurite Glasses Handbook, Physical Properties and Data, Second Edition, CRC Press, 2012.

[2] M.Dolhen, M.Tanaka, V.Couderc, S.Chenu, G.Delaizir, T.Hayakawa, J.Cornette, M.Colas, P.Thomas, J.-R.Duclère, "Nd^{3+}-doped transparent polycrystalline tellurite ceramics", *Sci.Rep.* **8** (2018) 4640.

[3] H.Algarni, M.Reben, Y.M.AbouDeif, K.Damak, A.A.Assadi, R.Maãlej, E.S.Yousef, "Thermal and spectroscopic properties of high dense optical glasses TeO_2-Bi_2O_3-WO_3 (TBW) doped with Er_2O_3 as laser material", *Sci.Adv.Mater.* **10** (2018) 1-9.

[4] A.Bertrand, J.Carreaud, S.Chenu, M.Allix, E.Veron, J-R.Duclère, Y.Launay, T.Hayakawa, C.Genevois, F.Brisset, F.Célarié, P.Thomas, G.Delaizir, "Scalable and formable tellurite-based transparent ceramics for near infrared applications", *Adv. Opt. Mater.* **4**(10) (2016) 1482-1486.

[5] M.Hayakawa, T.Hayakawa, X.T.Zhang, M.Nogami, "Optical detection of near infrared femtosecond laser-heating of Er^{3+}-doped ZnO-Nb_2O_5-TeO_2 glass by green up-conversion fluorescence of Er^{3+} ions", *J.Lumin.* **131** (2011) 843-849.

[6] K.Kato, T.Hayakawa, Y.Kasuya, P.Thomas, "Influence of Al_2O_3 incorporation on the third-order nonlinear optical properties of Ag_2O-TeO_2 glasses", *J.Non-Cryst. Solids* **431**(1) (2016) 97-106.

[7] V.P.Tuyen, B.Sengthong, V.X.Quang, P.V.Doc, H.V.Tuyen, L.X.Hung, N.T.Thanh, M.Nogami, T.Hayakawa, B.T.Huy, "Dy^{3+} ions as optical probes for studying structure of boro-tellurite glasses", *J. Lumin.* **178** (2016) 27-33.

[8] A. Bertrand, J. Carreaud, G. Delaizir, M. Shimoda, J. R. Duclère, M. Colas, M. Belleil, J. Cornette, T. Hayakawa, C. Genevois, E. Veron, M. Allix, F. Brisset, P. Thomas, "New transparent glass-ceramics based on the crystallization of "anti-glass" spherulites in the Bi_2O_3-Nb_2O_5-TeO_2 system", *Cryst. Growth Des.* **15**(10) (2015) 5086-5096.

[9] Y.G. Choi, J.Heo, "1.3mm emission and multiphonon relaxation phenomena in PbO-Bi_2O_3-Ga_2O_3 glasses doped with rare-earths", *J.Non-Cryst.Solids* **217** (1997) 199-207.

[10] C.B.Layne, W.H.Lowdermilk, M.J.Weber, "Multiphonon relaxation of rare-earth ions in oxide glasses", *Phys.Rev.B* **16**(1) (1977) 10-20.

[11] M. Shimoda, M. Uchida, T. Hayakawa, P. Thomas, "Synthesis and glass-structure of transparent zinc–niobate-tellurite glasses with low hydroxyl impurities", *Ceram. Int.* **43**(3) (2017) 2962-2968.

[12] M.R.Zaki, D.Hamani, M.Dutreilh-Colas, J.-R.Duclere, O.Masson, P.Thomas, "Synthesis, thermal, structural and linear optical properties of new glasses within the TeO_2-TiO_2-WO_3 system", *J.Non-Cryst.Solids* **484** (2018) 139-148.

[13] M.Soulis, A.P.Mirgorodsky, T.Merle-Méjean, O.Masson, P.Thomas, M.Udovic, "The role of modifier's cation valence in structural properties of TeO_2-based glasses", *J.Non-Cryst. Solids* **354** (2008) 143-149.

[14] H.Bürger, K.Kneipp, H.Hobert, W.Vogel, V.Kozhukharov, S.Neov, "Glass formation, properties and structure of glasses in the TeO_2-ZnO system", *J.Non-Cryst.Solids* **151** (1992) 134-142.

[15] N.S.Tagiara, D.Palles, E.D.Simandiras, V.Psycharis, A.Kyritsis, E.I.Kamitsos, "Synthesis, thermal and structural properties of pure TeO_2 glass and zinc-tellurite glasses", *J.Non-Cryst. Solids* **457** (2017) 116-125.

[16] R.Rolli, K.Gatterer, M.Wachtler, M.Bettinelli, A.Speghini, D.Ajò, "Optical spectroscopy of lanthanide ions in ZnO-TeO_2 glasses", *Spectrochim. Acta A* **57**(10) (2001) 2009-2017.

[17] L.M.Moreira, V.Anjos, M.J.V.Bell, C.A.R.Ramos, L.R.P.Kassab, D.J.L.Doualan, P.Camy, R.Moncorgé, "The effects of Nd_2O_3 concentration in the laser emission of TeO_2-ZnO glasses", *Opt.Mater.* **58** (2016) 84-88.

[18] F.Cabello, S.Sanchez-Cortes, M.Jiménez de Castro, "Influence of the preparation conditions of erbium-doped bismuth germinate glasses on tis optical response", *J.Non-Cryst.Solids* **445-446** (2016) 110-115.

[19] S.-H.Kim, T.Yoko, S.Sakka, "Linear and nonlinear optical properties of TeO_2 glass", *J.Am.Ceram.Soc.* **76**(10) (1993) 2486-2490.

[20] E.R.Barney, A.C.Hannon, D.Holland, N.Umesaki, M.Tatsumisago, R.G.Orman, S.Feller, "Terminal oxygens in amorphous TeO_2", *J.Phys.Chem.Lett.* **4** (2013) 2312-2316.

[21] T.Fujiwara, T.Hayakawa, M.Nogami, J.R.Duclère, P.Thomas, "Optical properties and Judd-Ofelt parameters of Sm^{3+} doped $BiO_{1.5}$-WO_3-TeO_2 glasses", *Phys.Status Solidi* C **8**(9) (2011) 2597-2600.

[22] T.Hayakawa, M.Koduka, M.Nogami, J.R.Duclère, A.P.Mirgorodsky, P.Thomas, "Metal oxide doping effects on Raman spectra and third-order nonlinear susceptibilities of thallium-tellurite glasses", *Scr. Mater.* **62** (2010) 806-809.

[23] T.Hayakawa, T.Suhara, T.Fujiwara, M.Nogami, P.Thomas, "Raman spectra and third-order nonlinear optical Z-scan properties of MO-Nb_2O_5-TeO_2 (M=Zn, Mg, Ca, Sr, Ba) glasses", *Phys.Status Solidi* C **8**(9) (2011) 2633-2636.

[24] M.Uchida, T.Hayakawa, T.Suhara, J.R.Duclère, P.Thomas, "Tm^{3+} concentration dependence on blue up-conversion photoluminescence for Tm^{3+}/Yb^{3+} co-doped TeO_2-$TlO_{0.5}$-ZnO glasses", *Int. J. Appl. Glass Sci.* **6**(1) (2015) 83-93.

[25] Y.Li, Q.Zhang, J.Song, Z.Gao, W.Tang, A.Lu, "Glass formation and spectral studies of PbO and Bi_2O_3 modified TeO_2-ZnO glasses", *J.Non-Cryst.Solids* **483** (2018) 43-49.

[26] A.Marczewska, M.Sroda, M.Nocun, "Thermal and spectroscopic characterization of gallium-tellurite glasses doped BaF_2 and PbO", *J.Non-Cryst.Solids* **464** (2017) 104-114.

[27] A.Kaur, A.Khanna, L.I.Aleksandrov, "Structural, thermal, optical and photo-luminescent properties of barium tellurite glasses doped with rare-earth ions", *J.Non-Cryst.Solids* **476** (2017) 67-74.

[28] N.Ghribi, M.Colas, J.-R.Duclère, T.Hayakawa, J.Carreaud, R.Karray, A.Kabadou, P.Thomas,

"Thermal, optical and structural properties of glasses within the TeO_2-TiO_2-ZnO system", *J. Alloys Compd.* **622** (2015) 333-340.

[29] J.Tauc, G.Grigorovici, A.Vancu, "Optical properties and electronic structure and amorphous germanium", *Phys.Status Solidi* **15** (1966) 627-637.

[30] M.S.Shakeri, M.Rezvani, "Optical band gap and spectroscopic study of lithium alumino silicate glass containing Y^{3+} ions", *Spectrochim. Acta A* **79** (2011) 1920-1925.

[31] D.Lorenc, M.Aranyosiova, R.Buczynski, R.Stepien, I.Bugar, A.Vincze, D.Velic, "Nonlinear refractive index of multicomponent glasses designed for fabrication of photonic crystal fibers", *Appl.Phys. B* **93** (2008) 531-538.

[32] A.Hruby, "Evaluation of glass-formin gtendency by means of DTA", *Czech. J.Phys. B* **22** (1972) 1187-1193.

[33] M.Uchida, T.Hayakawa, T.Suhara, J.R.Duclère, P.Thomas, "Raman investigation and glass-compositional dependence on blue up-conversion photoluminescence for Tm^{3+}/Yb^{3+} co-doped TeO_2-$TlO_{0.5}$-ZnO glasses", *Opt.Mater.Express* **4**(4) (2014) 823-835.

[34] T.Sekiya, N.Mochida, A.Ohtsuka, M.Tonokawa, "Normal vibrations of two polymorphic forms of TeO_2 crystals and assignments of Raman peaks of pure TeO_2 glass", *J.Ceram.Soc. Japan* **97** (1989) 1435-1440.

[35] T.Sekiya, N.Mochida, A.Ohtsuka, M.Tonokawa, "Raman spectra of $MO_{1/2}$-TeO_2 (M=Li, Na, K. Rb, Cs and Tl) glasses", *J.Non-Cryst.Solids* **144** (1992) 128-144.

[36] T.Sekiya, N.Mochida, A.Ohtsuka, "Raman spectra of MO-TeO_2 (M=Mg,Sr, Ba and Zn) glasses", *J.Non-Cryst.Solids* **168** (1994) 106-114.

[37] H.Scholze, "Glass", Springer Verlag, Berlin, New York (1977).

[38] L.Nemec, J.Götz, "Infrared absorption of ON- in E glass", *J.Am.Ceram.Soc.* **53**(9) (1970) 526.

[39] K. Chida, F. Hanawa and M. Nakahara, "Fabrication of OH-free multi-mode fiber by vapor phase axial deposition", *IEEE J. Quant. Electron.* **QE-18** (1982) 1883-1889.

[40] B.R. Judd, "Optical absorption intensities of rare-earth ions," *Phys. Rev.* **127**(3), 750-761 (1962).

[41] G.S. Ofelt, "Intensities of crystal spectra of rare earth ions", *J. Chem. Phys.* **37**(3), 511-520 (1962).

[42] W.F.Krupke, "Induced-emission cross sections of Neodymium laser glasses", *IEEE J.Quant. Electron.* **QE-10**(4) (1974) 450-457.

[43] W.T.Carnall, P.R.Fields, K.Rajnak, "Spectral intensities of the trivalent lanthanides and actinides in solution. II. Pm^{3+}, Sm^{3+}, Eu^{3+}, Gd^{3+}, Tb^{3+}, Dy^{3+}, and Ho^{3+}", *J.Chem.Phys.* **49**(10) (1968) 4412-4423.

[44] W.T.Carnall, P.R.Fields, B.G.Wybourne, "Spectral intensities of the trivalent lanthanides and actinides in solution. I. Pr^{3+}, Nd^{3+}, Er^{3+}, Tm^{3+}, and Yb^{3+}", *J.Chem.Phys.* **42**(11) (1965) 3797-3806.

[45] W.T.Carnall, P.R.Fields, K.Rajnak, "Electric energy levels in the trivalent lanthanide aquo ions. I. Pr^{3+}, Nd^{3+}, Pm^{3+}, Sm^{3+}, Dy^{3+}, Ho^{3+}, Er^{3+}, and Tm^{3+}", *J.Chem.Phys.* **49**(10) (1968) 4424-4442.

[46] T.Schweizer, D.W.Hewak, B.N.Samson, D.N.Payne, "Spectroscopic data of the 1.8-, 2.9-, and

4.3-μm transitions of dysprosium-doped gallium lanthanum sulfide glass", *Opt.Lett.* **21** (19) (1996)1594-1596.

[47] G.Bilir, "Synthesis and spectroscopy of Nd^{3+}-doped tellurite-based glasses", *Int.J.Appl.Glass Sci.* **6**(4) (2015) 397-405.

[48] J.L.Liu, W.C.Wang, Y.B.Xiao, S.J.Huang, L.Y.Mao, Q.Y.Zhang, "Nd^{3+}doped TeO_2-MoO_3-ZnO tellurite glass for a diode-pump 1.06 μm laser", *J.Non-Cryst.Solids* **506** (2019) 32-38.

[49] S.Yu, Z.Yang, S.Xu, "Judd-Ofelt and laser parameterization of Tm^{3+}-doped barium gallo-germanate glass fabricated with efficient dehydration method", *Opt.Mater.* **31**(11) (2009) 1723-1728.

[50] Y.B.Shin, H.T.Lim, Y.G.Choi, Y.S.Kim. J.Heo, "2.0 μm emission properties and energy transfer between Ho^{3+} and Tm^{3+} in PbO-Bi_2O_3-Ga_2O_3 glasses", *J.Am.Ceram.Soc.* **83**(4) (2000) 787-791.

[51] J.Fábry, J.Loub, L.Feltl, "A study of the thermal decompositions of orthotelluric acid, urea and the orthotelluric acid adduct with urea", *J.Therm.Analy.* **24** (1982) 95-100.

[52] E.De la Rosa-Cruz, G.A.Kumar, L.A.Diaz-Torres, A.Martínez, O.Barbosa-García, "Spectroscopic characterization of Nd^{3+} ions in barium fluoroborophosphate glasses", *Opt.Mater.* **18** (2001) 321-329.

[53] M.J.Bell, V.Anjos, L.M.Moreira, R.F.Falci, L.R.P.Kassab, D.S.da Silva, J.L.Doualan, P.Camy, R.Moncorgé, "Laser emission of a Nd-doped mixed tellurite and zinc oxide glass", *J.Opt.Soc.Am.B* **31**(7) (2014) 1590-1594.

[54] M.M.Mann, L.G.DeShazer, "Energy levels and spectral broadening of neodymium ions in laser glass", *J.Appl.Phys.* **41**(7) (1970) 2951-2957.

[55] A.Miguel, J.Azkargorta, R.Morea, I.Iparraguirre, J.Gonzalo, J.Fernandez, R.Balda, "Spectral study of the stimulated emission of Nd^{3+} in fluorotellurite bulk glass", *Opt.Exp.* **21**(8) (2013) 9298-9307.

[56] R.Balda, J.Fernández, M.A.Arriandiaga, J.M.Fernández-Navarro, "Spectroscopy and frequency upconversion in Nd^{3+}-doped TeO_2-TiO_2-Nb_2O_5 glass", *J.Phys.:Condens.Matter* **19** (2007) 086223 (12pp).

[57] H.Kalaycioglu, H.Cankaya, G.Ozen, L.Ovecoglu, A.Sennaroglu, "Lasing at 1065 nm in bulk Nd^{3+}-doped telluride tungstate glass", *Opt.Commun.* **281** (2008) 6056-6060.

[58] K.Upendra Kumar, V.A.Prathyusha, P.Babu, C.K.Jayasankar, A.S.Joshi, A.Speghini, M.Bettinelli, "Fluorescence properties of Nd^{3+}doped tellurite glasses", *Spectrochim. Acta* A **67** (2007) 702-708.